PNAS RESEARCH ARTICLE | PHARMACOLOGY

Targeted recruitment of immune effector cells for rapid eradication of influenza virus infections

Imrul Shahriar[a,b,1], Mohini Kamra[a,2], Ananda Kumar Kanduluru[a,b], Charity Lynn Campbell[a,b], Thanh Hiep Nguyen[c], Madduri Srinivasarao[a,b], and Philip S. Low[a]

Affiliations are included on p. 9.

Edited by Peter Palese, Icahn School of Medicine at Mount Sinai, New York, NY; received April 28, 2024; accepted July 19, 2024

Despite much research, considerable data suggest that influenza virus remains a serious health problem because i) the effectiveness of current vaccines ranges only from 19% to 60%, ii) available therapies remain ineffective in advanced stages of disease, iii) death rates vary between 25,000 and 72,000/year in the United States, and iv) avian influenza strains are now being transmitted to dairy cattle that in turn are infecting humans. To address these concerns, we have developed zanDR, a bispecific small molecule that binds and inhibits viral neuraminidase expressed on both free virus and virus-infected cells and recruits naturally occurring anti-rhamnose and anti-dinitrophenyl (DNP) antibodies with rhamnose and DNP haptens. Because the neuraminidase inhibition replicates the chemotherapeutic mechanism of zanamivir and oseltamivir, while rhamnose and DNP recruit endogenous antibodies much like an anti-influenza vaccine, zanDR reproduces most of the functions of current methods of protection against influenza virus infections. Importantly, studies on cells in culture demonstrate that both of the above protective mechanisms remain highly functional in the zanDR conjugate, while studies in lethally infected mice with advanced-stage disease establish that a single intranasal dose of zanDR not only yields 100% protection but also reduces lung viral loads faster and ~1,000× more thoroughly than current antiviral therapies. Since zanDR also lowers secretion of proinflammatory cytokines and protects against virus-induced damage to the lungs better than current therapies, we suggest that combining an immunotherapy with a chemotherapy in single pharmacological agent constitutes a promising approach for treating the more challenging forms of influenza.

antiviral therapeutics | immunotherapy of influenza virus infections | recruitment of antibodies to virus-infected cells

Significance

Concerns over periodic influenza pandemics remain high, primarily because current therapies are ineffective in treating advanced stages of disease and generally less effective in treating avian influenza virus strains against which we have little or no immunity. To address these concerns, we have designed a bispecific small molecule (zanDR) that both inhibits influenza virus neuraminidase and recruits the immune system, thereby reducing the viral load in lethally infected mice much faster and more effectively (~1,000×) than any current therapy. With the ability of influenza virus to infect and mutate in animals before transmission to humans, efforts to integrate an immunotherapy and chemotherapy into a single small molecule with intranasal bioavailability warrant investigation to further enhance our pandemic preparedness.

Although familiarity with influenza virus might mollify public concerns over influenza's enduring risk, influenza virus infections still cause 35-65 million illnesses, 16 to 30 million medical visits, 390,000 to 830,000 hospitalizations, and 25,000 to 72,000 deaths/year in the United States, resulting in more fatalities than acute myelogenous leukemia, hemorrhagic stroke, AIDS caused by HIV, or ovarian cancer (1–4). While FDA-approved drugs such as oseltamivir, zanamivir, and baloxavir are effective when administered early during an infection, they become ineffective in later stages of disease, emphasizing the need for a therapy that can treat more severe infections (5–7). Moreover, if one of the many virulent avian strains were to mutate to infect humans, lack of preexisting immunity and the absence of an effective treatment could trigger a pandemic of serious proportions (8–10). Clearly, a need exists for a more potent, strain-agnostic influenza virus therapy.

Although vaccines have proven pivotal in the battle against influenza, their impact has been mitigated by the fact that only half of all Americans exhibit immunity at any one time, either because they have not been vaccinated or have allowed their immunities to lapse (11, 12). To address these challenges, we have designed a low-molecular-weight bifunctional molecule that both inhibits viral replication and recruits immune effector cells to kill both free virus and virus-infected host cells. In this strategy, an established influenza virus neuraminidase inhibitor (zanamivir) is linked to two different haptens against which naturally occurring antibodies exist in virtually all humans. Upon administration to a patient, the neuraminidase inhibitor moiety of the bifunctional molecule binds to viral neuraminidase on both infectious virions and virus-infected cells, thereby inhibiting viral proliferation by the mechanism previously established for zanamivir (13). Concurrently, the two attached haptens recruit endogenous anti-hapten antibodies, thereby decorating the virions/virus-infected cells with naturally occurring immunoglobulins that in turn induce removal of the opsonized viruses/infected cells by Fc receptor–expressing immune cells (14–30). Importantly, while use of a single hapten was previously found to be

Competing interest statement: I.S. and M.S. receive consulting fees from Eradivir Inc., A.K.K. and C.L.C. are employees at Eradivir Inc., and P.S.L. serves on the board of directors of Eradivir Inc. P.S.L., A.K.K., M.S., I.S., and M.K. are listed as inventors on a relevant patent filing (Patent No. WO2023205669A3)

This article is a PNAS Direct Submission.

[1]To whom correspondence may be addressed. Email: ishahria@purdue.edu.

[2]Present address: Department of Biomedical Engineering, The University of Texas at Austin, Austin, TX 78712.

This article contains supporting information online at https://www.pnas.org/lookup/suppl/doi:10.1073/pnas.2408469121/-/DCSupplemental.

Published September 30, 2024.

insufficient to protect severely infected unimmunized mice (31), incorporation of the second hapten is now demonstrated to enable rapid elimination of 10^3 times more virus than zanamivir, oseltamivir, or baloxavir alone. Because this dual hapten conjugate can promote complete protection in mice even when initiation of therapy is delayed for 96 h postinoculation with 10× half-maximal lethal dose (LD_{50}) of influenza virus, and since the bifunctional conjugate can induce potent antiviral immune effector functions without causing any toxicity, we conclude that this combination chemotherapy plus immunotherapy constitutes a promising mechanism for treatment of influenza virus infections.

Results

Design of the Zanamivir-Dual-Hapten Conjugate (zanDR) for Treatment of Influenza Virus Infections. Motivated by promising data on the use of tumor-targeted haptens to treat cancers (14–17, 19–21, 23, 24, 26–29, 32–38), we have undertaken to design a targeted hapten immunotherapy for the treatment of influenza virus infections that not only exploits the therapeutic potency of an established viral neuraminidase inhibitor (i.e., zanamivir) but also recruits the immune system in a manner related to an anti-influenza vaccine (Fig. 1*A*). Because a single targeted hapten (dinitrophenyl; DNP) was found to be incapable of curing infected mice that are not immunized against DNP (31), we incorporated a second hapten into our zanamivir conjugate against which even higher titers of naturally occurring antibodies exist in virtually all humans (Fig. 1*A*), thereby facilitating recruitment of a much larger repertoire of endogenous anti-hapten antibodies. We hypothesized that if endogenous anti-hapten antibody titers were sufficiently high, decoration of hapten-coated viral particles/virus-infected cells with anti-hapten antibodies would initiate an immune response that together with the accompanying neuraminidase inhibition would successfully treat even the most severe influenza virus infections. The studies described below test this hypothesis in mice inoculated with ten times the LD_{50} of influenza virus.

Analysis of Anti-Hapten Antibody Titers in Humans. Although a number of naturally occurring anti-hapten antibodies have been identified in virtually all humans, we have focused our efforts on anti-rhamnose and anti-DNP antibodies since they are reported to be two of the most abundant in humans and their haptens are readily available (19, 29, 30, 39, 40). To quantify the titers of these antibodies in human individuals, we purchased 133 deidentified human serum samples from BioIVT that were collected from 94 healthy volunteers, 29 influenza patients, and 10 healthy infants, and measured their anti-DNP and anti-rhamnose antibody titers, as described in *Materials and Methods*. As shown in Fig. 1*B* and

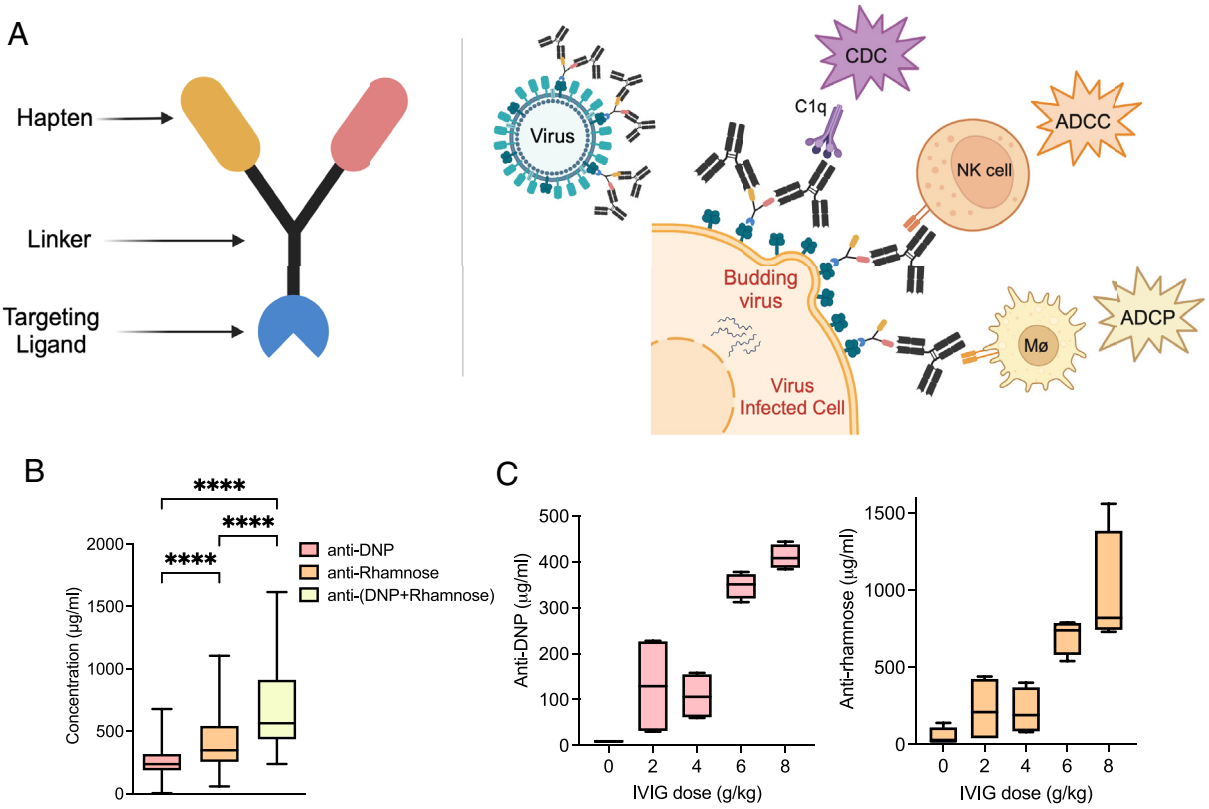

Fig. 1. Hypothesized structure and mechanism of action of zanDR, a dual-action antiviral agent, and mimicking human-like anti-hapten antibody titer in mice for therapeutic evaluation of zanDR. (*A*) Schematic representation of the structure of the dual-action antiviral therapeutic agent (zanDR; *Left* panel) and its hypothesized mechanism of action (*Right* panel). As depicted in the *Right* panel, the zanamivir moiety in zanDR binds to the viral neuraminidase on both free virus and virus-infected host cells and the attached haptens recruit endogenous anti-hapten antibodies that trigger removal of the virions and virus-infected cells by Fc receptor expressing immune cells and the complement system. (*B* and *C*) Quantification of anti-DNP and anti-rhamnose antibody titers in human serum samples (panel *B*) and murine serum samples (N = 4/cohort) after infusion of human IVIG (panel *C*). Human serum samples (N = 133) were analyzed by the ELISA for their concentrations of anti-DNP and anti-rhamnose antibody titers, as described in *Materials and Methods*. The total anti-DNP + anti-rhamnose titers were calculated by simply summing the data for each individual antibody titer in each sample. Statistical differences between anti-DNP, anti-rhamnose, and anti-(DNP+Rhamnose) groups were determined by ordinary one-way ANOVA (****$P < 0.0001$) in GraphPad Prism 10. Unmodified human intravenous immunoglobulin (IVIG) was infused intraperitoneally into live mice, and the resulting anti-DNP and anti-rhamnose antibody titers were determined 24 h after injection (n = 4 mice/group). The data are plotted with the default box and whiskers plotting feature in GraphPad Prism 10. The box extends from the 25th to 75th percentiles. The line in the middle of the box is plotted at the median. The whiskers go down to the smallest value and up to the largest. The limit of detection (LoD) for anti-DNP antibody titer is 0.23 µg/mL and for anti-rhamnose antibody titer is 0.16 µg/mL.

SI Appendix, Fig. S1, anti-DNP titers averaged ~260 μg/mL, while anti-rhamnose titers averaged ~423 μg/mL. Because all 133 serum samples contained both anti-DNP and anti-rhamnose antibodies, and since their titers did not decrease significantly with age nor vary between males and females, or between healthy and infected individuals (*SI Appendix*, Fig. S1), we conclude that incorporation of both a rhamnose and DNP hapten into a zanamivir-targeted conjugate should assure that any patient who might fortuitously suffer from a low level of one antibody should still receive protection from the other.

Mimicking Human-Like Anti-Hapten Antibody Titers in Mice. Because mice have few anti-DNP and anti-rhamnose antibodies, in order to test our hypothesis in a murine model, we determined the amount of unfractionated human IgG that would have to be transfused into a mouse to replicate the anti-hapten antibody titers found in humans. For this purpose, mice were injected intraperitoneally with increasing concentrations of human IVIG, and blood samples were collected 24 h later for quantification of antibody titers. As shown in Fig. 1*C*, injection of 6 g/kg human IVIG approximated the average anti-DNP and anti-rhamnose antibody titers measured in humans. Therefore, 6 g/kg human IVIG was first cleared of endogenous anti-influenza antibodies (*Materials and Methods*) and then injected intraperitoneally into mice to mimic the anti-hapten antibody titers normally found in humans.

Characterization of the Mechanism of Action of Zanamivir-DNP-Rhamnose (zanDR) Conjugate In Vitro. In order to characterize the properties of the dual hapten zanamivir-DNP-rhamnose conjugate (hereafter termed zanDR); (see synthesis in *SI Appendix*, Schemes S1–S3), we first compared the affinity of zanDR and unmodified zanamivir for influenza virus neuraminidase (N1) to ensure that attachment of the two haptens would not significantly interfere with its neuraminidase-binding ability. As shown in Fig. 2*A*, zanDR bound to influenza virus neuraminidase-transduced Human Embryonic Kidney 293 (HEK293) cells with an affinity of ~10 nM, i.e., similar to that of a zan-rhodamine conjugate. Moreover, because binding of zanamivir conjugates to the neuraminidase-expressing HEK293 cells could be quantitatively blocked with unmodified zanamivir, we conclude that association of zanDR with the transduced HEK293 cells was solely neuraminidase mediated.

To assess the ability of zanDR to treat influenza virus strains that might express different subtypes of neuraminidase, we next evaluated its ability to inhibit the neuraminidase activities of five of the more common strains of influenza virus [A/PR/8/1934 (H1N1), A/Wisconsin/15/2009 (H3N2), A/California/04/2009 (H1N1pdm09), B/Brisbane/60/2008 (Victoria Lineage), and A/Hong Kong/2369/2009 (H1N1pdm09, oseltamivir resistant)]. As shown in Fig. 2*B*, zanDR retained the capacity to inhibit all five neuraminidases, including a subtype (A/Hong Kong/2369/2009) that is known to be oseltamivir-resistant. Although it was not feasible to test zanDR against the more dangerous strains of influenza virus (41), we can nevertheless conclude that zanDR's neuraminidase-binding ability should be sufficiently broad to enable its targeting of haptens and inhibition of neuraminidase activities in the viral strains commonly encountered today.

Next, to evaluate the ability of zanDR to recruit sufficient naturally occurring anti-hapten antibodies to mediate ADCC- and CDC-induced killing of virus-infected cells, we transduced HEK293 cells with influenza virus neuraminidase and examined the ability of zanDR to promote ADCC and CDC killing of the neuraminidase-expressing cells. As shown in Fig. 2*C*, zanDR was effective in mediating ADCC of the neuraminidase-transduced HEK293 cells, displaying the anticipated bell-shaped dependence on zanDR concentration (42). Moreover, the fact that this killing could be blocked by either in the absence of neuraminidase expression or competition with 100-fold excess free zanamivir confirmed that ADCC killing required cell surface expression of influenza virus neuraminidase. This latter requirement is important since it establishes that uninfected cells should not be damaged by zanDR.

Not surprisingly, zanDR was also found to promote CDC-mediated killing of neuraminidase-expressing target cells (Fig. 2 *C*, *Right* panel), and this killing was also blocked by 100-fold excess free zanamivir, i.e., confirming that zanDR-mediated activation of complement-mediated killing should also be limited to cells/virions that express viral neuraminidase.

Dose Optimization and Efficacy of zanDR in a Murine Model of Influenza Virus Infection. Because the impact of ADCC and CDC on therapeutic efficacy can best be evaluated in vivo, we next determined the survival of mice infected with 10× LD_{50} of the A/PR/8/1934 (H1N1) strain of influenza virus following initiation of treatment 96 h postinfection (96 hpi). For purposes of comparison, similarly infected mice were treated intravenously with phosphate-buffered saline (PBS) (control), 1.5 μmol/kg of zanDR (with or without prior IVIG administration), 1.5 μmol/kg zanamivir-dinitrophenyl single hapten conjugate (zanDNP), or 1.5 μmol/kg zanamivir-rhamnose single hapten conjugate (zan-rhamnose). Moreover, to achieve the anti-DNP and anti-rhamnose titers found in humans, all mice including those in the PBS control group were infused at 72 hpi with 6 g/kg human IVIG to mimic the anti-hapten antibody titers chronically found in humans (see above). As shown in Fig. 3*A*, treatment with intravenous zanDR (with IVIG) yielded 100% protection, while injection of either zan-DNP or zan-rhamnose promoted only 80% and 60% survival, respectively, i.e., confirming that attachment of two haptens improves potency. The zanDR-treated cohort that did not receive IVIG prior to drug administration resulted in only 40% survival, indicating that the presence of the anti-hapten antibodies led to the recruitment of immune effector cells which in turn protected the mice from infection-induced mortality. Importantly, treatment with unmodified zanamivir alone also yielded 40% protection, and administration of PBS alone produced no survivors. Because all mice (including those treated with PBS alone) rapidly lost 15 to 20% of their body weight, we concluded that the lethal dose of virus likely caused the weight loss, and this assumption was confirmed when the zanDR-treated groups rapidly regained their normal body weights.

To obtain an estimate of the minimal zanDR concentration required for complete protection of the lethally infected mice, additional cohorts of the same mice were treated with 0, 0.17, 0.5, 1.5, or 4.5 μmol/kg of zanDR and analyzed for survival. As shown in panel *B*, all mice in the higher two concentration cohorts achieved complete protection, while survival of mice in the lower three cohorts decreased to 40%, 20%, and 0%, respectively. Again, although significant body weight loss was observed in all cohorts, zanDR-treated groups regained their body weights ~8 dpi, while no mice in the placebo control group survived the challenge beyond this 8 dpi. Based on these data, we conclude that a single dose of 1.5 μmol/kg zanDR constitutes the minimal dose required to protect mice infected with 10× LD_{50} A/PR/8/1934 (H1N1) when treatment is delayed for 96 h postinfection.

Because zanamivir can be administered to patients intranasally (43), it became important to determine whether zanDR might also be administered intranasally. To address this question, mice were treated intravenously (IV) or intranasally (IN) with 1.5 μmol/kg zanDR, and blood samples were collected at the intervals

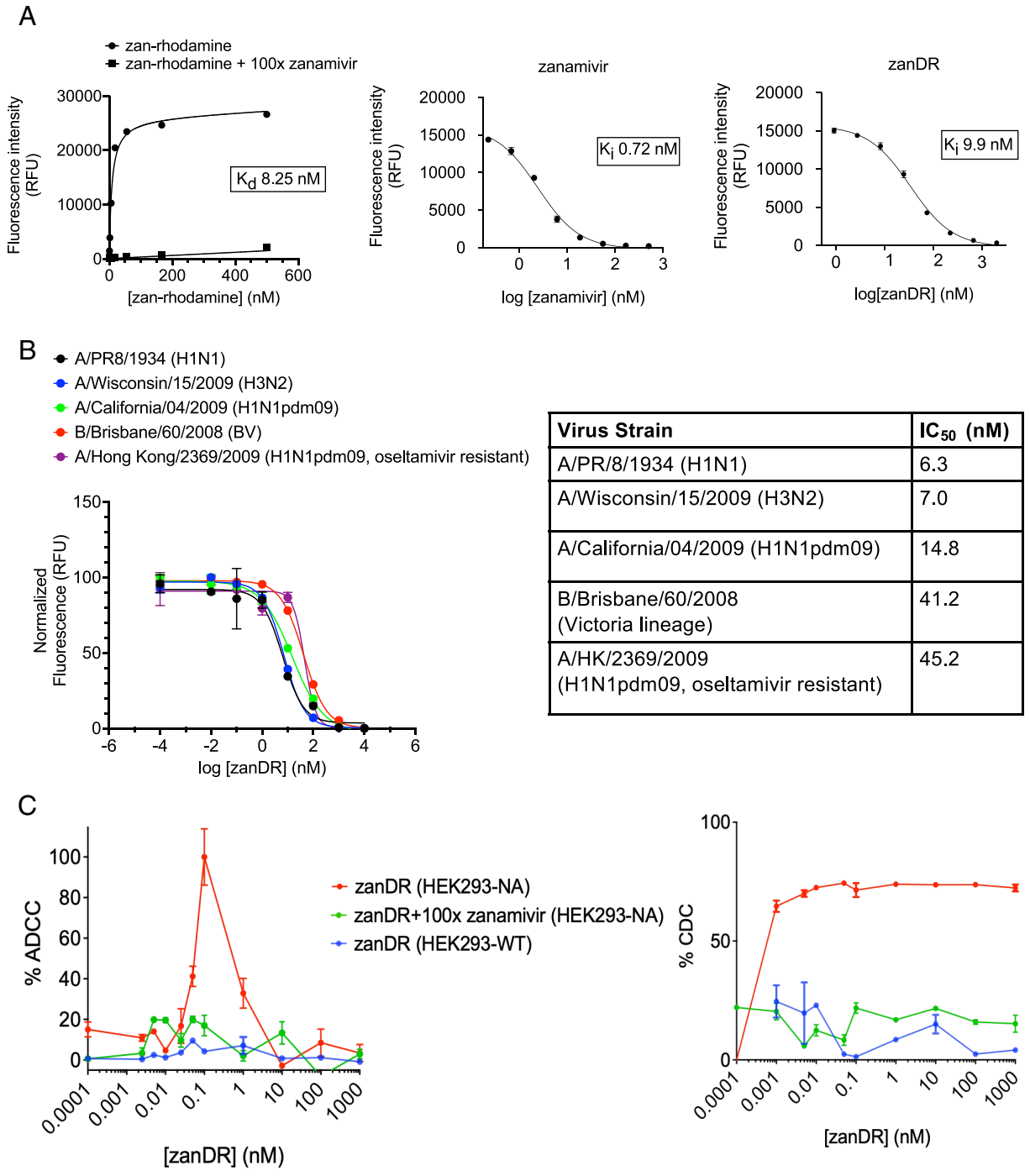

Virus Strain	IC_{50} (nM)
A/PR/8/1934 (H1N1)	6.3
A/Wisconsin/15/2009 (H3N2)	7.0
A/California/04/2009 (H1N1pdm09)	14.8
B/Brisbane/60/2008 (Victoria lineage)	41.2
A/HK/2369/2009 (H1N1pdm09, oseltamivir resistant)	45.2

Fig. 2. Evaluation of the binding and functional properties of zanDR in vitro. (*A*) Analysis of the binding affinity of zanDR and the zan-rhodamine conjugate for N1 neuraminidase-expressing HEK293 cells. (*Left* panel) Direct binding of increasing concentrations of zan-rhodamine to HEK293-N1 cells. (*Central* and *Right* panels) Concentration-dependent inhibition of zan-rhodamine binding to HEK293-N1 neuraminidase cells by increasing concentrations of free zanamivir (*Central* panel) or zanDR (*Right* panel). The assay was performed in triplicates (N = 3). (*B*) Binding of zanDR to multiple influenza virus strains was quantified by evaluating its ability to inhibit the neuraminidase expressed on the surfaces of these different virus particles. The assay was performed in duplicates (N = 2). (*C*) Evaluation of the ability of zanDR to mediate killing of HEK293 cells induced to express N1 neuraminidase by either antibody-dependent cellular cytotoxicity (ADCC) or complement-dependent cytotoxicity (CDC). For this study, the HEK293-N1-neuraminidase cell cultures were supplemented with IVIG or human serum and incubated with serial dilutions of zanDR in the presence or absence of 100× zanamivir. All assays were performed in duplicate (N = 2), and all error bars indicate the SEM.

shown in *SI Appendix*, Fig. S2. Significantly, zanDR was highly bioavailable following IN administration, exhibiting an area under the curve (AUC) that was 76% of the AUC achieved following IV injection. While C_{max} was admittedly lower after IN infusion, the drug persisted longer in circulation (*SI Appendix*, Fig. S2) and weight loss due to infection was dramatically reduced (Fig. 3*C*). Because patient compliance might also be enhanced by IN administration, IN administration was used in all further studies.

To compare the potency of zanDR with current treatments for influenza virus infections, we again infected mice with 10× LD_{50} A/PR/8/1934 (H1N1) and treated them 96 h later, only this time the mice were administered PBS, 1.5 μmol/kg zanDR, or the commonly used literature doses of baloxavir, zanamivir, or oseltamivir (44, 45). All mice in the PBS and zanDR cohorts received 6 g/kg IVIG intraperitoneally at 72 hpi. As shown in Fig. 3*C*, all mice treated with zanDR survived, whereas only 60%, 40%, 20%, and

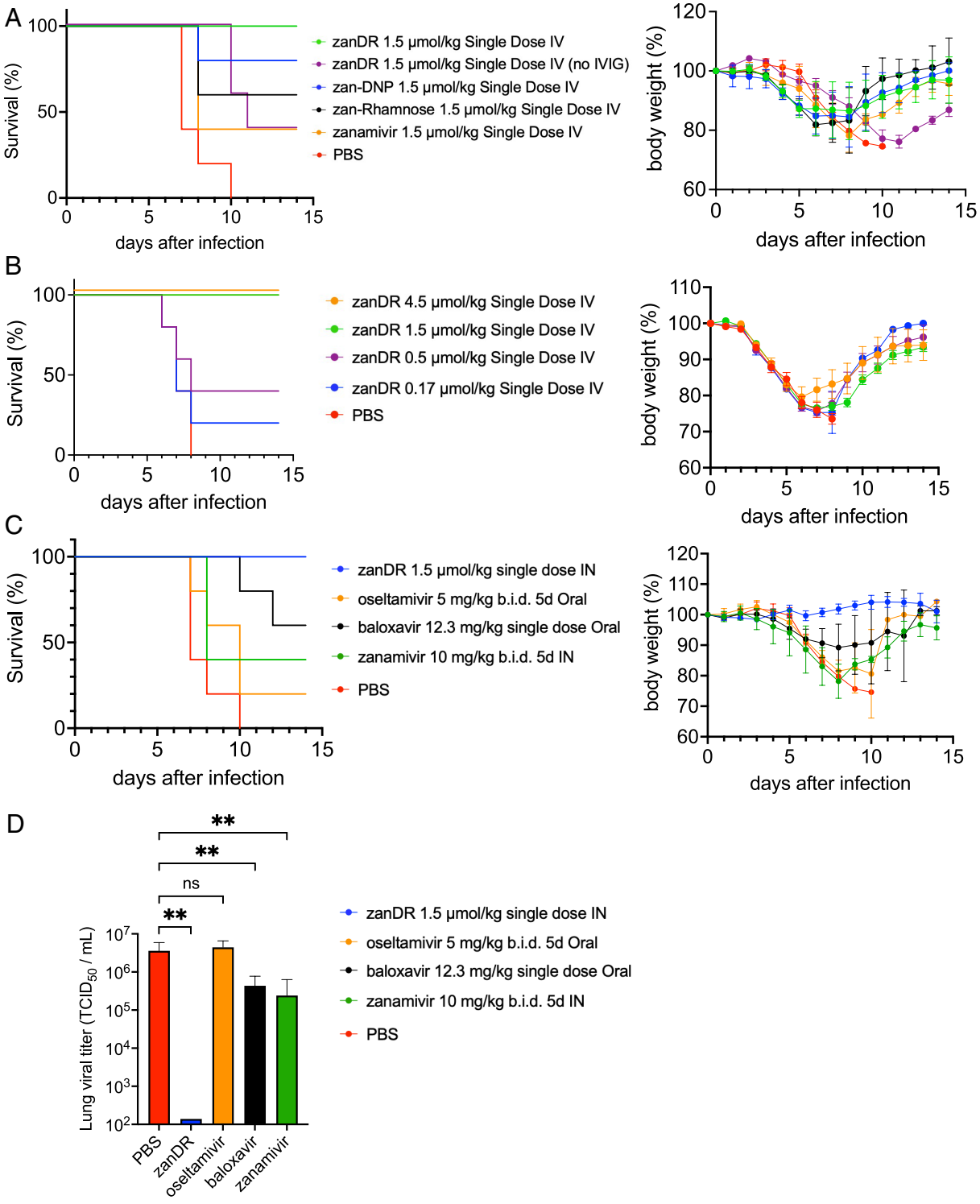

Fig. 3. In vivo efficacy evaluation studies with zanDR. (*A*) Comparison of the survival of mice (N = 5/cohort) infected with 10× LD_{50} titers of H1N1 influenza virus following treatment with the indicated concentrations of zanDR, zan-DNP, zan-rhamnose, unmodified zanamivir alone, or PBS. All mice in the zanDR, zan-DNP, zan-rhamnose, and the PBS groups received 6 g/kg of IVIG intraperitoneally at 72 hpi. The zanDR cohort received zanDR without IVIG administration. Statistical differences among the survival curves were assessed using a log-rank (Mantel–Cox) test (*P* value 0.0013, significant difference) and Gehan–Breslow–Wilcoxon test (*P* value 0.0024, significant difference) in GraphPad Prism 10. (*B*) Dose range finding study in 6- to 8-wk-old female BALB/c mice (N = 5/cohort) infected with 10× LD_{50} titers of influenza A/PR/8/1934 (H1N1) virus following treatment with the indicated concentrations of zanDR administered as a single dose IV injection. All experimental cohorts received 6 g/kg of IVIG intraperitoneally including the PBS control group at 72 hpi. Statistical differences among the survival curves were assessed using a log-rank (Mantel–Cox) test (*P* value 0.0035, significant difference) and Gehan–Breslow–Wilcoxon test (*P* value 0.0070, significant difference) in GraphPad Prism 10. (*C*) Comparison of the survival of mice (N = 5/cohort) infected with 10× LD_{50} titers of H1N1 influenza virus following treatment with the indicated concentrations of zanDR (1.5 μmol/kg single dose, intranasal), oseltamivir phosphate (5 mg/kg twice daily for 5 d), baloxavir marboxil (12.3 mg/kg single dose, oral), or zanamivir (10 mg/kg, twice daily for 5 d). Mice in the zanDR cohort and in the PBS control group received 6 g/kg IVIG intraperitoneally at 72 hpi. Survival curves (*Left* panels) and body weight curves (*Right* panels) for each treatment cohort are shown. Body weights of mice that died from the infection were not included in subsequent body weight averages. Statistical differences among the survival curves were assessed using a log-rank (Mantel–Cox) test (*P* value 0.0002, significant difference) and Gehan–Breslow–Wilcoxon test (*P* value 0.0003, significant difference) in GraphPad Prism 10. (*D*) Quantification of the viral titers remaining in the lungs of H1N1 infected mice (N = 5/cohort) 24 h after treatment with the indicated therapies. Statistical analysis was performed by ordinary one-way ANOVA and Dunnett's multiple comparisons test. The *P* values for PBS vs. zanDR, oseltamivir, baloxavir, and zanamivir are 0.0028(**), 0.7635(ns), 0.0084(**), and 0.0051(**), respectively. All the error bars in the figure indicate the SEM.

0% of mice treated with baloxavir, zanamivir, oseltamivir, and PBS survived. These data not only establish the unusual antiviral potency of zanDR but also demonstrate that recruitment of the immune system plays a prominent role in the efficacy of zanDR.

Finally, to obtain a more quantitative estimate of the relative potencies of zanDR, zanamivir, baloxavir, and oseltamivir, we again infected mice as above and treated them 96 h later with the same drugs (panel *D*), only this time the mice were killed 24 h after drug administration and peripheral blood and lung tissues were removed for quantification of their virus contents. As shown in panel *D*, PBS-treated mice contained live influenza virus titers in their lungs of ~4×10^6 half-maximal tissue culture infectious dose ($TCID_{50}$)/mL, whereas titers in the lungs of oseltamivir-, zanamivir-, and baloxavir-treated mice were ~4×10^6, 2.2×10^5, and ~3.7×10^5 $TCID_{50}$/mL, respectively. Importantly, influenza virus in the zanDR-treated mice was not detectable, suggesting that the infectious virions had been significantly reduced in all extracellular and intracellular compartments. Because these differences in residual titers following therapy with zanDR- and the neuraminidase inhibitors exceeded 3 orders of magnitude, we conclude that the hapten-mediated (immunotherapy) component of zanDR's mechanism of action makes a greater contribution to overall potency than the neuraminidase-inhibiting component.

Treatment with zanDR Is Accompanied by Little or no Systemic Inflammation. Because both expansion and elimination of an influenza virus infection can trigger an inflammatory response, leading to fever, headache, sore throat, and body pain (46), and

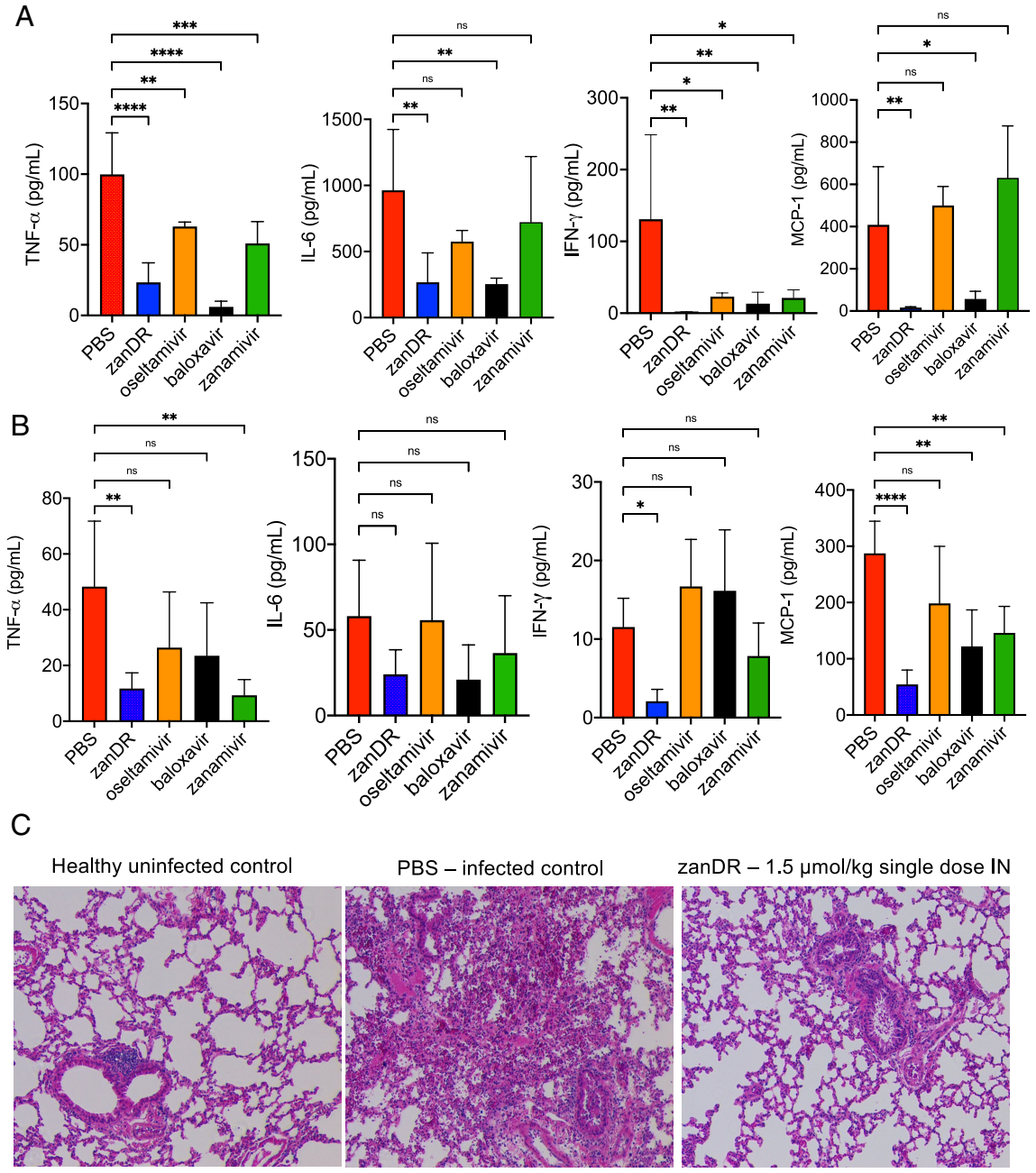

Fig. 4. Comparison of potential toxicity parameters following treatment with the indicated influenza therapies. Concentrations of the major inflammatory cytokines were measured in the lungs (*A*) and peripheral blood (*B*) of mice (N = 5/cohort) in each treatment cohort. Statistical analysis was performed by ordinary one-way ANOVA and Dunnett's multiple comparisons test (P values are depicted as 0.1234(ns), 0.0032(*), 0.0021(**), 0.0002(***), and <0.0001(****). (*C*) Representative thin sections of the lungs (N = 5/cohort) of each treatment group were imaged following H&E staining. All the error bars in the figure indicate the SEM.

since excessive immune activation can lead to immunopathology or pneumonia (47), the data in Fig. 3*D* invite the question of whether zanDR's reduction of such a large number of viruses in very short (24-h) time might cause intolerable inflammation-mediated toxicity. To obtain an initial assessment of this possible problem, we compared the level of cytokines released following treatment with zanDR with those induced after administration of oseltamivir, baloxavir, and zanamivir. For this purpose, whole blood and lung samples were collected and analyzed for inflammatory cytokines immediately after killing of animals. As shown in Fig. 4, levels of Tumor Necrosis Factor alpha (TNFα), Interferon gamma (IFNγ), Interleukin 6 (IL-6), and Monocyte Chemoattractant Protein 1 (MCP-1) were all lower in both the lungs (panel *A*) and peripheral blood (panel *B*) of therapeutically treated animals than in PBS-treated controls, revealing that inflammation-related toxicities must be less in the treated than untreated animals. This remarkable absence of obvious zanDR-induced toxicity was further established by comparison of the micrographs obtained from the infected lungs of the same animals. As shown in panel *C*, diffuse alveolar damage, pulmonary edema, and excessive inflammatory cell infiltration were evident in the PBS-treated controls, whereas the same parameters were greatly reduced in the zanDR-treated cohort. Overall, the data suggest that administration of zanDR reduces rather than increases damage to the influenza virus-infected lungs.

Potential Application of zanDR in Treating Drug-Resistant Influenza Virus Infections. Aside from the inability of current antiviral drugs to treat advanced influenza virus infections, a rising concern lies in their possible inabilities to treat drug-resistant strains of influenza virus (48–51). Fortunately, emergence of zanamivir-resistant strains has been rare, probably because zanamivir's structure is very similar to that of sialic acid, i.e., the substrate that influenza virus neuraminidase must cleave for the virus to proliferate (52). As a consequence, all oseltamivir-resistant strains to date have remained susceptible to zanamivir, i.e., suggesting that zanDR might also retain its efficacy against oseltamivir-resistant influenza virus strains. Nevertheless, to evaluate this hypothesis, we infected mice with 2.8× LD_{50} of the oseltamivir-resistant strain, A/Hong Kong/2369/2009 (H1N1pdm09, H275Y), and then treated the mice with zanDR, oseltamivir, or PBS control at 24 hpi as depicted in Fig. 5. While oseltamivir showed no improvement in survival over PBS-treated controls, a single intranasal dose of zanDR yielded 100% protection with no significant animal weight loss. These data suggest that zanDR may be more resistant to the emergence of drug-resistant strains of influenza virus than most other therapies.

Discussion

The fact that ~55% of individuals suffering from influenza virus infections recover without medical intervention suggests that the immune system can readily eliminate the majority of influenza virus infections without pharmaceutical countermeasures (4). This endogenous resistance can largely be attributed to the presence of natural antibodies, particularly Immunoglobulin G (IgG), which are abundant in the lower respiratory tract and play a crucial role in neutralizing viruses, activating complement, and facilitating opsonization, thereby enhancing the body's ability to combat influenza virus infections (53, 54). In this study, we have coopted the remarkable potency of the immune system to augment the activity of a repurposed FDA-approved neuraminidase inhibitor (zanamivir) by linking zanamivir to two orthologous haptens against which all humans have antibodies. When administered intranasally or intravenously, this zanamivir-dual-hapten conjugate (zanDR) recruits endogenous anti-hapten antibodies onto virions and virus-infected cell surfaces, thereby triggering removal of both pathogenic components. That this recruitment of antibodies provides the major contribution to therapeutic efficacy was documented by two observations, namely that 1) all three neuraminidase inhibitors (i.e., oseltamivir, zanamivir, baloxavir) lowered viral titers 24 h after administration by only 0- to 100-fold, whereas zanDR reduced titers by >10,000-fold, and 2) zanDR prevented all mice from dying due to infection with 10× LD_{50} influenza virus, whereas oseltamivir, zanamivir, and baloxavir only promoted survival of 20%, 40%, and 60% of the same infected mice.

Motivated by the likely improved patient compliance with an intranasal route of administration, we elected to test whether zanDR might prove effective following intranasal administration. Surprisingly, the IN-infused drug not only reduced viral titers more potently but also inhibited animal weight loss better than its IV-infused counterpart. While some flow of zanDR directly into the infected lungs might account for part of this improved potency, it should still be noted that zanDR must cross an epithelial cell barrier to gain access to anti-rhamnose and anti-DNP antibodies in the blood that are responsible for the immunotherapeutic component of efficacy. Perhaps the improved pharmacokinetics of the intranasally administered drug might enable more prolonged access to virus and virus-infected cells than the intravenously administered drug.

Recognizing that an overactive immune system can cause harm to healthy tissues and noting the speed with which zanDR reduced severe influenza virus infections, we looked for signs of immune-related toxicities following zanDR administration. As noted in Fig. 4, not only were cytokine levels reduced and lung tissue

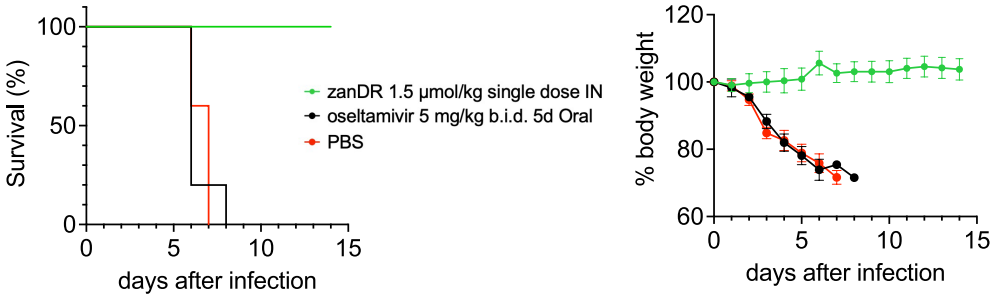

Fig. 5. Comparison of the abilities of zanDR and oseltamivir to treat an infection with an oseltamivir-resistant strain of influenza virus. Comparison of the survival of BALB/c mice (N = 5/cohort) infected with 2.8× LD_{50} titers of A/Hong Kong/2369/2009 (H1N1pdm) (H275Y, Oseltamivir Resistant) strain following treatment with the indicated concentrations of zanDR, oseltamivir phosphate, and PBS (*Left* panel). Mice in the zanDR cohort and in the PBS control group received 6 g/kg IVIG intraperitoneally at 0 hpi as zanDR was administered at 24 hpi. Impact of the treatment regimens on mouse body weight (*Right* panel). The statistical difference between the survival curves was assessed using a log-rank (Mantel–Cox) test (*P* value 0.0005, significant difference) and Gehan–Breslow–Wilcoxon test (*P* value 0.0011, significant difference) in GraphPad Prism 10. All the error bars in the figure indicate the SEM.

traumas mitigated in intranasally treated mice, but animal weight losses were also suppressed. While this outcome initially seemed counterintuitive, we later realized that zanDR-mediated killing was restricted to viral neuraminidase-expressing cells/virions, which should have constituted only a fraction of the cells in the lungs. Thus, unlike many other immunotherapies, where the targeted antigen can also be expressed on healthy cells, the absence of influenza virus neuraminidase on normal cells (31) can apparently protect the patient from significant damage to healthy tissues.

In conclusion, zanDR may represent a significant advance in the development of more potent therapies for influenza virus infections. The ability of zanDR to redirect endogenous anti-hapten antibodies toward infectious virions/infected cells offers a promising approach to treat patients who delay seeking medical intervention until their infections are no longer responsive to current therapies. While efficacy was clearly demonstrated against an oseltamivir-resistant strain, the suspected transmission of avian influenza virus from a cow to a human (55) emphasizes the need to both expand and accelerate research efforts toward broader and more potent therapies for influenza virus. Based on the data presented here, an immunotherapeutic component with the efficacy of an antibody in the size of a small molecule should be considered for inclusion in any such therapy.

Materials and Methods

Enzyme-Linked Immunosorbent Assay (ELISA) for Quantification of Anti-DNP and Anti-Rhamnose Antibody Titers. To quantify the titers of anti-DNP and anti-rhamnose antibodies in humans, we purchased human serum samples from BioIVT. All the samples were deidentified by the vendor, and no personally identifiable information was disclosed. ELISA plates (Fisher Scientific) were coated with 5 μg/mL bovine serum albumin (BSA)-2,4-dinitrophenyl (DNP) solution (Invitrogen) or BSA-Rhamnose solution (Dextra) in 1× ELISA coating buffer (BioLegend). After three washes with 1× ELISA wash buffer (BioLegend), plates were blocked with ELISA Assay Diluent (BioLegend) for 45 min. Serial 10-fold dilutions of purified human polyclonal IgG were used to generate standard curves (please see *SI Appendix* for the purification method). After incubation with standard or test samples for 1 h, wells were washed with 1X ELISA Wash buffer (BioLegend). Following four washes, wells were exposed to anti-human IgG-horseradish peroxidase (HRP)/anti-mouse IgG-HRP (1:5,000 in blocking buffer, Invitrogen) for 45 min. After four additional washes, plates were treated with 3,3′,5,5′-tetramethylbenzidine (TMB) substrate solution (BioLegend) for 10 min. Enzymatic reactions were stopped, and optical density was measured at 450 nm using a Synergy Neo2 HTS Multi-Mode Microplate Reader (Biotek). Anti-DNP and anti-rhamnose antibody titers in human/mouse serum samples were determined using the standard curve, and GraphPad Prism 10 was used for generating the titer distribution plots.

IVIG Dose Optimization Study in Mice. Six- to eight-week-old female Bagg albino (BALB)/c mice (n = 6/group) were injected intraperitoneally with 0, 2, 4, 6, or 8 g/kg human IVIG (Gamunex®-C 10%, Grifols, 50 mL vial), and blood samples were collected from the submandibular (facial) vein of mice. Samples were then centrifuged at 2,000×*g* for 10 min in a refrigerated centrifuge at 4 °C to obtain the mouse serum to determine the anti-DNP and anti-rhamnose IgG antibody titers according to the ELISA protocol described above.

Competitive Binding Assay. zanDR's binding affinity (K_i) was assessed via a competitive binding assay using a zanamivir-rhodamine (zan-rhodamine) conjugate as a fluorescent probe. Initially, the zanamivir-rhodamine conjugate's dissociation constant (K_d) with influenza virus neuraminidase (N1) expressing HEK293 cells (HEK293-N1) was determined. HEK293-N1 cells were plated and treated with serial dilutions of zan-rhodamine in the presence or absence of 100× excess zanamivir for determination of nonspecific binding. After incubation and washing, fluorescence intensity was measured using the Attune NxT Flow Cytometer, and K_d was calculated in GraphPad Prism 10 (saturation binding equations, one site – total and nonspecific binding).

zanDR's inhibitory constant (K_i) was determined alongside zanamivir as a positive control. Serial dilutions of zanDR and zanamivir were mixed with the zanamivir-rhodamine conjugate, added to HEK293-N1 cells, incubated, and washed, and fluorescence intensity was measured at the end of the assay. Utilizing the previously calculated K_d and a fixed concentration of the zan-rhodamine conjugate, K_i values were computed using GraphPad Prism 10 (competitive binding equations, one site – Fit K_i).

Viral Neuraminidase Inhibition Assay. To assess zanDR's neuraminidase inhibition activity, the NA-Fluor™ Influenza Neuraminidase Assay Kit (Invitrogen™) was employed following the manufacturer's protocol. Briefly, a standard curve generated with 4-methylumbelliferone sodium salt [4-MU(SS)] determined the linear range for fluorescence detection on a Synergy Neo2 HTS Multi-Mode Microplate Reader. Virus stock solutions were titrated through a neuraminidase activity assay using serial dilutions in a 96-well black-walled plate. The chosen dilution factor for each virus strain, corresponding to a predetermined relative fluorescence unit (RFU) value from the standard curve, was then used for normalization in the neuraminidase inhibition assay. In the neuraminidase inhibition assay, tenfold serial dilutions of the test compounds were prepared in NA-Fluor™ assay buffer. A 4× zanDR dilution series and diluted virus samples were added to the designated wells of a 96-well black-walled plate, incubated for 30 min at 37 °C, and then treated with the NA-Fluor™ substrate. After incubating for 60 min, fluorescence intensities were measured, and data were analyzed using GraphPad Prism 10 to generate sigmoid dose–response curves. The built-in nonlinear regression curve-fitting program was used to determine the half-maximal inhibitory concentration (IC_{50}) of zanDR.

Evaluation of the Antibody-Dependent Effector Functions in Vitro. To test the proof of concept of the mechanism of action of zanDR in vitro, ADCC and CDC assays were performed. The ADCC assay was performed using a commercially available ADCC Reporter Bioassay kit (Promega, cat. no. G7010; Promega Corporation, Madison, WI) with influenza virus neuraminidase (N1)-transfected (NA-HEK) cells as the target cells. For this purpose, cells were plated in triplicate (100 μL, 5,000 cells/well) in 96-well black-walled plates (Corning Life Sciences, Corning, NY) and then treated with serial dilutions of zanDR in the presence or absence of 100-fold excess zanamivir. After incubating at 37 °C for 2 h, human IVIG was added to each well, and the plates were incubated at 37 °C for another 2 h. Finally, ADCC effector cells were added at 75,000 cells/well and incubated overnight at 37 °C under 5% CO_2. The amount of firefly luciferase produced by the ADCC bioassay effector cells (human FcγRIIIa expressing cells) through nuclear factor of activated T cell (NFAT) response was then quantified using Bio-Glo™ luciferase assay reagent (included in the kit). Luminescence was measured using the Synergy Neo2 HTS Multi-Mode Microplate Reader (BioTek Instruments).

For the CDC assay, N1-transfected (NA-HEK) cells were harvested and plated in triplicate (100 μL, 5,000 cells/well) in 96-well black-walled plates (Corning Life Sciences, Corning, NY) and then treated with serial dilutions of zanDR in the presence or absence of 100-fold excess of zanamivir. After incubating at 37 °C for 2 h, human serum was added to each well, and the plates were incubated overnight at 37 °C under 5% CO_2. Cell viability was measured using the Cell Titer 96 Aqueous Non-Radioactive Cell Proliferation Assay (Promega Corporation, Madison, WI).

Animal Experiment Design. The half-maximal lethal dose defined as the viral inoculation required to kill 50% of the infected mice in a survival challenge study (LD_{50}) was determined as described in a previous article from our group (31). For the dose-range finding study, 6- to 8-wk-old female BALB/c mice (n = 5/cohort) were challenged intranasally with 10× LD_{50} of Influenza A/Puerto Rico/8/1934 (H1N1) virus under isoflurane anesthesia. The mice were administered a 6 g/kg intraperitoneal injection of human IVIG (Gamunex®-C, Grifols) 24 h prior to administration of zanDR. The PBS control group received IVIG at the same timepoint as well to ensure that they had the same background IVIG as the mice that were treated with zanDR. Two lots of Gamunex®-C 10% (Grifols) (50 mL each) were procured from a local pharmacy. Mice were given an intranasal dose of different concentrations of zanDR at 96 h postinfection under isoflurane anesthesia. The mice were weighed and observed daily for a period of 14 d following infection. If they lost 25% of their body weight or were determined to

be moribund, they were considered deceased and killed according to the animal protocol approved by the Institutional Animal Care and Use Committee (IACUC). For the in vivo efficacy comparison studies, mice were infected and infused with IVIG as described above. Different concentrations of the respective test articles were administered at 96 h postinfection, and the mice were monitored as described above for survival analysis and body weight loss measurements. For in vivo efficacy evaluation against the oseltamivir-resistant influenza virus strain, mice were infected with 2.8× LD_{50} titers of A/Hong Kong/2369/2009 (H1N1pdm) (H275Y, oseltamivir resistant) and treated with test articles at 24 h postinfection and monitored as described above for survival analysis and weight loss measurements.

Quantification of Lung Viral Titers. Mouse lungs were homogenized in 5 μL of cold 1× PBS per milligram of tissue. All samples were stored at −80 °C. For determining the half-maximal tissue culture infectious dose ($TCID_{50}$), MDCK-London (Madin-Darby Canine Kidney, London Line) cells were plated in a 96-well plate and incubated till confluent. On the day of the assay, lung lysate was serially diluted threefold in Dulbecco's Modified Eagle Medium/Nutrient Mixture F-12 (DMEM/F12) (1:1) supplemented with 0.3% BSA. MDCK-London cells were washed, and 50 μL of diluted lysate was added to each well so that each dilution had four replicates. Cells were incubated for 1 h at 37 °C, 5% CO_2, and then, 200 μL of DMEM/F12 (1:1) supplemented with 0.3% BSA and 1 μg/mL of L-(tosylamido-2-phenyl) ethyl chloromethyl ketone (TPCK)-treated trypsin was added to each well. Cells were incubated for 48 h at 37 °C and 5% CO_2. Each well was tested for hemagglutination by incubating 50 μL of tissue culture supernatant with 50 μL of 0.5% turkey red blood cells in phosphate-buffered saline in a V-bottom plate. After 30 min of incubation at room temperature, the plate was tilted 45 degrees, and wells were counted as negative or positive. Negative wells had a red dot, that ran when the plate was tilted, resembling the negative control. Positive wells appeared hazy and did not have a red dot at the bottom of the well. $TCID_{50}$ was calculated for each lung sample using the Reed–Muench method, and values were plotted using GraphPad Prism 10.

Quantification of Inflammatory Cytokines. Levels of the major inflammatory cytokines in the lungs and serum of influenza virus-infected mice were measured 24 h posttreatment. Blood samples were collected from five mice per cohort, and then, the mice were killed to isolate the lung tissues. Lungs were homogenized in 5 μL of cold PBS per milligram of tissue, and 100 μL of lysate was mixed with 100 μL of 2× protease inhibitor buffer followed by centrifugation at 800×*g* and 4 °C for 5 min to remove cell debris. BioLegend's LEGENDplex™ bead-based immunoassay was used to determine the cytokine levels using the standard protocol provided by the manufacturer (BioLegend, San Diego, CA). Fluorescence intensities were measured using an Attune NxT flow cytometer (ThermoFisher Scientific), and the concentration of each inflammatory marker was quantified using LEGENDplex™ software (BioLegend). Finally, data were plotted with GraphPad Prism 10.

Histopathological Evaluation. Twenty-four hours after drug administration (120 h postinfection), mice were subjected to isoflurane anesthesia followed by cervical dislocation. Lung tissues were fixed in 10% neutral buffered formalin (NBF), embedded in paraffin, sectioned, and stained with hematoxylin and eosin (H&E), and then imaged under a Nikon Eclipse light microscope at 10× magnification.

Pharmacokinetic Analysis of zanDR in Mice. Six- to eight-week-old female BALB/c mice (3 mice/group) were administered with a single intravenous (IV) or intranasal (IN) dose of 1.5 μmol/kg of zanDR, and blood samples were collected at 5 min, 30 min, 1 h, 2 h, 4 h, and 8 h after drug administration. The plasma concentration of zanDR was determined by liquid chromatography with tandem mass spectrometry (LC–MS/MS). IVIG was administered as the source of anti-hapten antibodies 24 h prior to drug administration. The pharmacokinetic parameters were calculated using PKSolver (56).

Statistical Analyses. Statistical analyses were performed using GraphPad Prism 10 (GraphPad Software, CA). For comparative analysis of the lung viral titers and the major inflammatory cytokines in the serum and lungs, statistical difference between the groups were determined using ordinary one-way ANOVA and Dunnett's multiple comparisons test. For all the mouse therapy studies, the statistical difference between the survival curves was assessed using a log-rank (Mantel–Cox) test and Gehan–Breslow–Wilcoxon test.

Data, Materials, and Software Availability. All study data are included and directly available in the article and/or supporting information.

ACKNOWLEDGMENTS. We acknowledge the use of the Chemical Genomics Facility, a core facility of Purdue Institute for Drug Discovery, and facilities of the Bindley Bioscience Center and the NIH-funded Indiana Clinical and Translational Sciences Institute. We are grateful to Dr. Brett Hurst and Dr. Bart Tarbet from the Institute of Antiviral Research, Utah State University, UT, for kindly providing the oseltamivir-resistant influenza virus strain. We are grateful to Dr. Katherine A. Wall for kindly providing the purified anti-rhamnose antibodies.

Author affiliations: [a]James Tarpo Jr. and Margaret Tarpo Department of Chemistry, Purdue University, West Lafayette, IN 47907; [b]Eradivir Inc., West Lafayette, IN 47906; and [c]Department of Biological Sciences, Purdue University, West Lafayette, IN 47907

Author contributions: I.S., M.K., A.K.K., M.S., and P.S.L. designed research; I.S., M.K., A.K.K., C.L.C., and T.H.N. performed research; I.S., M.K., A.K.K., C.L.C., and T.H.N. analyzed data; and I.S. and P.S.L. wrote the paper.

1. R. L. Siegel, K. D. Miller, N. S. Wagle, A. Jemal, Cancer statistics, 2023. *CA Cancer J. Clin.* **73**, 17–48 (2023).
2. S. N. Poisson, D. Glidden, S. C. Johnston, H. J. Fullerton, Deaths from stroke in US young adults, 1989–2009. *Neurology* **83**, 2110 (2014).
3. HIV & AIDS trends and U.S. statistics overview. HIV.gov. https://www.hiv.gov/hiv-basics/overview/data-and-trends/statistics/. Accessed 20 February 2024.
4. 2023–2024 U.S. flu season: Preliminary in-season burden estimates. CDC. https://www.cdc.gov/flu/about/burden/preliminary-in-season-estimates.htm. Accessed 23 March 2024.
5. S. G. Muthuri *et al.*, Effectiveness of neuraminidase inhibitors in reducing mortality in patients admitted to hospital with influenza A H1N1pdm09 virus infection: A meta-analysis of individual participant data. *Lancet Respir. Med.* **2**, 395–404 (2014).
6. L. M. Koonin, A. Patel, Timely antiviral administration during an influenza pandemic: Key components. *Am. J. Public Health* **108**, S215 (2018).
7. What you should know about flu antiviral drugs. CDC. https://www.cdc.gov/flu/treatment/whatyoushould.htm. Accessed 11 November 2023.
8. Technical Report: Highly pathogenic avian influenza A(H5N1) viruses. https://www.cdc.gov/flu/avianflu/spotlights/2022-2023/h5n1-technical-report_october.htm. Accessed 11 November 2023.
9. C. Adlhoch *et al.*, Avian influenza overview December 2022–March 2023. *EFSA J.* 21, e07917 (2023).
10. CDC A(H5N1) bird flu response update June 14, 2024. Bird Flu. CDC (2024). https://www.cdc.gov/bird-flu/spotlights/h5n1-response-06142024.html. Accessed 14 June 2024.
11. Flu vaccination coverage, United States, 2022–23 influenza season. FluVaxView. Seasonal Influenza (Flu). CDC. https://www.cdc.gov/flu/fluvaxview/coverage-2223estimates.htm. Accessed 11 November 2023.
12. CDC seasonal flu vaccine effectiveness studies. CDC. https://www.cdc.gov/flu/vaccines-work/effectiveness-studies.htm. Accessed 11 November 2023.
13. M. Elliott, Zanamivir from drug design to the clinic. *Philos. Trans. R. Soc. Lond. B, Biol. Sci.* **356**, 1885–1893 (2001).
14. R. P. Murelli, A. X. Zhang, J. Michel, W. L. Jorgensen, D. A. Spiegel, Chemical control over immune recognition: A class of antibody-recruiting small molecules that target prostate cancer. *J. Am. Chem. Soc.* **131**, 17090–17092 (2009).
15. A. Dubrovska *et al.*, A chemically induced vaccine strategy for prostate cancer. *ACS Chem. Biol.* **6**, 1223–1231 (2011).
16. A. F. Rullo *et al.*, Re-engineering the immune response to metastatic cancer: Antibody-recruiting small molecules targeting the urokinase receptor. *Angew. Chem. Int. Ed. Engl.* **55**, 3642–3646 (2016).
17. S. M. Rathmann *et al.*, A versatile platform for the development of radiolabeled antibody-recruiting small molecules. *Mol. Pharm.* **18**, 2647–2656 (2021).
18. N. Hribernik, F. Chiodo, R. J. Pieters, A. Bernardi, Rhamnose-based glycomimetic for recruitment of endogenous anti-rhamnose antibodies. *Tetrahedron Lett.* **99**, 153843 (2022).
19. R. T. C. Sheridan, J. Hudon, J. A. Hank, P. M. Sondel, L. L. Kiessling, Rhamnose glycoconjugates for the recruitment of endogenous anti-carbohydrate antibodies to tumor cells. *ChemBioChem* **15**, 1393 (2014).
20. Y. Lu, P. S. Low, Folate targeting of haptens to cancer cell surfaces mediates immunotherapy of syngeneic murine tumors. *Cancer Immunol. Immunotherapy* **51**, 153–162 (2002).
21. E. I. Sega, Y. Lu, M. Ringor, C. P. Leamon, P. S. Low, Low-dose radiation potentiates the therapeutic efficacy of folate receptor-targeted hapten therapy. *Int. J. Radiat. Oncol. Biol. Phys.* **71**, 559–566 (2008).
22. Y. S. Yi, W. Ayala-López, S. A. Kularatne, P. S. Low, Folate-targeted hapten immunotherapy of adjuvant-induced arthritis: Comparison of hapten potencies. *Mol. Pharm.* **6**, 1228–1236 (2009).
23. Y. Lu *et al.*, Folate-targeted dinitrophenyl hapten immunotherapy: Effect of linker chemistry on antitumor activity and allergic potential. *Mol. Pharm.* **4**, 695–706 (2007).

24. N. A. Bandara, C. D. Bates, Y. Lu, E. K. Hoylman, P. S. Low, Folate-hapten-mediated immunotherapy synergizes with vascular endothelial growth factor receptor inhibitors in treating murine models of cancer. *Mol. Cancer Ther.* **16**, 461–468 (2017).
25. C. G. Parker, R. A. Domaoal, K. S. Anderson, D. A. Spiegel, An antibody-recruiting small molecule that targets HIV gp120. *J. Am. Chem. Soc.* **131**, 16392–16394 (2009).
26. K. Zhou *et al.*, Chemical synthesis of antibody-hapten conjugates capable of recruiting the endogenous antibody to magnify the Fc effector immunity of antibody for cancer immunotherapy. *J. Med. Chem.* **65**, 323–332 (2022).
27. B. Schrand *et al.*, Hapten-mediated recruitment of polyclonal antibodies to tumors engenders antitumor immunity. *Nat. Commun.* **9**, 3348 (2018).
28. P. J. McEnaney, C. G. Parker, A. X. Zhang, D. A. Spiegel, Antibody-recruiting molecules: An emerging paradigm for engaging immune function in treating human disease. *ACS Chem. Biol* **7**, 1139 (2012).
29. W. Chen *et al.*, L-rhamnose antigen: A promising alternative to α-gal for cancer immunotherapies. *ACS Chem. Biol.* **6**, 185–191 (2011).
30. C. E. Jakobsche *et al.*, Exploring binding and effector functions of natural human antibodies using synthetic immunomodulators. *ACS Chem. Biol.* **8**, 2404–2411 (2013).
31. X. Liu *et al.*, A universal dual mechanism immunotherapy for the treatment of influenza virus infections. *Nat. Commun.* **11**, 1–14 (2020).
32. E. Kapcan *et al.*, Covalent stabilization of antibody recruitment enhances immune recognition of cancer targets. *Biochemistry* **60**, 1447–1458 (2021).
33. B. P. M. Lake, R. G. Wylie, C. Bařinka, A. F. Rullo, Tunable multivalent platform for immune recruitment to lower antigen expressing cancers. *Angew. Chem. Int. Ed.* **62**, e202214659 (2023).
34. Y. Lu *et al.*, Preclinical pharmacokinetics, tissue distribution, and antitumor activity of a folate-hapten conjugate–targeted immunotherapy in hapten-immunized mice. *Mol. Cancer Ther.* **5**, 3258–3267 (2006).
35. N. A. Bandara, Immunotherapy of folate receptor expressing cancers. Theses and Dissertations Available from ProQuest (2015).
36. R. T. C. Sheridan, J. Hudon, J. A. Hank, P. M. Sondel, L. L. Kiessling, Rhamnose glycoconjugates for the recruitment of endogenous anti-carbohydrate antibodies to tumor cells. *ChemBioChem* **15**, 1393–1398 (2014).
37. R. J. Amato *et al.*, A Phase I/Ib study of folate immune (EC90 vaccine administered with GPI-0100 adjuvant followed by EC17) with interferon-α and interleukin-2 in patients with renal cell carcinoma. *J. Immunother.* **37**, 237–244 (2014).
38. R. J. Amato, A. Shetty, Y. Lu, R. Ellis, P. S. Low, A phase I study of Folate immune therapy (EC90 vaccine administered with GPI-0100 adjuvant followed by EC17) in patients with renal cell carcinoma. *J. Immunother.* **36**, 268–275 (2013).
39. O. Oyelaran, L. M. McShane, L. Dodd, J. C. Gildersleeve, Profiling human serum antibodies with a carbohydrate antigen microarray. *J. Proteome Res.* **8**, 4301–4310 (2009).
40. S. M. Muthana, J. C. Gildersleeve, Factors affecting anti-glycan IgG and IgM repertoires in human serum. *Sci. Rep.* **6**, 1–11 (2016).
41. Influenza type A viruses. Avian influenza (Flu). https://www.cdc.gov/flu/avianflu/influenza-a-virus-subtypes.htm. Accessed 7 March 2024.
42. E. F. Douglass, C. J. Miller, G. Sparer, H. Shapiro, D. A. Spiegel, A comprehensive mathematical model for three-body binding equilibria. *J. Am. Chem. Soc.* **135**, 6092 (2013).
43. D. P. Calfee, A. W. Peng, E. K. Hussey, M. Lobo, F. G. Hayden, Safety and efficacy of once daily intranasal zanamivir in preventing experimental human influenza A infection. *Antivir. Ther.* 4, 143–149 (1999).
44. K. Fukao *et al.*, Baloxavir marboxil, a novel cap-dependent endonuclease inhibitor potently suppresses influenza virus replication and represents therapeutic effects in both immunocompetent and immunocompromised mouse models. *PLoS ONE* **14**, e0217307 (2019).
45. D. F. Smee, M. Von Itzstein, B. Bhatt, E. B. Tarbet, Exacerbation of influenza virus infections in mice by intranasal treatments and implications for evaluation of antiviral drugs. *Antimicrob. Agents Chemother.* **56**, 6328 (2012).
46. L. Kaiser, R. S. Fritz, S. E. Straus, L. Gubareva, F. G. Hayden, Symptom pathogenesis during acute influenza: Interleukin-6 and other cytokine responses. *J. Med. Virol.* **64**, 262–268 (2001).
47. F. Krammer *et al.*, Influenza. *Nat. Rev. Dis.* **4**, 3 (2018).
48. T. Lampejo, Influenza and antiviral resistance: An overview. *Eur. J. Clin. Microbiol. Infect. Dis.* **39**, 1201–1208 (2020).
49. E. C. Holmes *et al.*, Understanding the impact of resistance to influenza antivirals. *Clin. Microbiol. Rev.* **34**, 1–13 (2021).
50. G. A. Poland, R. M. Jacobson, I. G. Ovsyannikova, Influenza virus resistance to antiviral agents: A plea for rational use. *Clin. Infect. Dis.* **48**, 1254 (2009).
51. D. F. Smee, J. G. Julander, E. Bart Tarbet, M. Gross, J. Nguyen, Treatment of oseltamivir-resistant influenza A (H1N1) virus infections in mice with antiviral agents. *Antiviral. Res.* **96**, 13 (2012).
52. A. Moscona, Oseltamivir resistance–Disabling our influenza defenses. *N. Engl. J. Med.* **353**, 2633–2636 (2005), 10.1056/NEJMp058291.
53. M. Koutsakos *et al.*, Assessment of antibodies in the upper and lower human respiratory tract at steady state and after respiratory viral infection. *Clin. Transl. Immunol.* **12**, e1460 (2023).
54. K. B. Renegar, P. A. Small, L. G. Boykins, P. F. Wright, Role of IgA versus IgG in the control of influenza viral infection in the murine respiratory tract. *J. Immunol.* **173**, 1978–1986 (2004).
55. Highly pathogenic avian influenza A (H5N1) virus infection reported in a person in the U.S. CDC Online Newsroom. CDC. https://www.cdc.gov/media/releases/2024/p0401-avian-flu.html. Accessed 19 April 2024.
56. Y. Zhang, M. Huo, J. Zhou, S. Xie, PKSolver: An add-in program for pharmacokinetic and pharmacodynamic data analysis in Microsoft Excel. *Comput. Methods Programs Biomed.* **99**, 306–314 (2010).